Published in final edited form as:
J Hypertens. 2009 October ; 27(10): 2010–2021. doi:10.1097/HJH.0b013e32832e8dc8.

IMPORTANCE OF PULSATILITY IN HYPERTENSIVE CAROTID ARTERY GROWTH AND REMODELING

J.F. Eberth[a], **V.C. Gresham**[b], **A.K. Reddy**[c], **N. Popovic**[d], **E. Wilson**[d], and **J.D. Humphrey**[a,*]

[a] Department of Biomedical Engineering and M.E. DeBakey Institute, Texas A&M University, College Station, TX

[b] Comparative Medicine Program, Texas A&M University, College Station, TX

[c] Section of Cardiovascular Sciences, Department of Medicine, Baylor College of Medicine, Houston, TX

[d] Department of Systems Biology and Translational Medicine, Texas A&M Health Science Center, College Station, TX

Abstract

Arteries experience marked variations in blood pressure and flow during the cardiac cycle that can intensify during exercise, in disease, or with aging. Diverse observations increasingly suggest the importance of such pulsatility in arterial homeostasis and adaptations. We used a transverse aortic arch banding model to quantify chronic effects of increased pulsatile pressure and flow on wall morphology, composition, and biaxial mechanical properties in paired mouse arteries: the highly pulsatile right common carotid artery proximal to the band (RCCA-B) and the nearly normal left carotid artery distal to the band (LCCA-B). Increased pulsatile mechanical stimuli in RCCA-B increased wall thickness compared to LCCA-B, which correlated stronger with pulse ($r^*=0.632$; $p<0.01$) than mean ($r^*=0.020$; $p=0.47$) or systolic ($r^*=0.466$; $p<0.05$) pressure. Similarly, inner diameter at mean pressure increased in RCCA-B and correlated slightly stronger with a normalized index of blood velocity pulsatility ($r^*=0.915$; $p \ll 0.001$) than mean flow ($r^*=0.834$; $p<0.001$). Increased wall thickness and luminal diameter in RCCA-B resulted from significant increases in cell number per cross-sectional area ($p<0.001$) and collagen to elastin ratio ($p<0.05$) as well as a moderate (1.7-fold) increase in glycosaminoglycan content, which appear to have contributed to the significant decrease ($p<0.001$) in the *in vivo* axial stretch in RCCA-B compared to LCCA-B. Changes in RCCA-B also associated with a signficant increase in monocyte chemoattractant protein-1 ($p<0.05$). Pulsatile pressure and flow are thus important stimuli in the observed three-dimensional arterial adaptations, and there is a need for increased attention to the roles of both axial wall stress and adventitial remodeling.

Introduction

The mammalian heart pumps blood through rhythmic contractions of varying magnitude and frequency depending on demand. Healthy large (central) arteries dampen out pulsations and help deliver continuous blood flow to distal tissue despite experiencing cyclic loading with each cardiac beat [1,2]. Different conditions hinder the ability of large arteries to dampen pulse pressure, however, including stiffening of the arterial wall that occurs in aging, atherosclerosis,

*Address for Correspondence: J.D. Humphrey, Department of Biomedical Engineering, 337 Zachry Engineering, Center, Texas A&M University, College Station, TX 77843-3120; Email: jhumphrey@tamu.edu; Phone: +1.979.845.5558; Fax: +1.979.845.4450.

Disclosures: None

or hypertension [1,3–5]. Indeed, pulse pressure related cyclic fatigue now appears to contribute to the degradation of elastin in aging and multiple diseases, and thus to the vicious cycle of stiffening and increased propagation of the pulse wave [5–10]. Patients with elevated pulse pressure are more susceptible to cardiovascular disease than those with only elevated mean blood pressure [11–14], hence there is a need for more attention to the effects of pulsatility on the arterial wall. Boutouyrie *et al.* [15] showed, for example, that increased pulse, not mean, pressure correlates better with enlargement and thickening of hypertensive carotid arteries in patients. Similarly, Guyton and Hartley [16] found in an animal model that altered carotid caliber correlates with changes in peak velocity and an index of pulsatility, but not mean flow. Nevertheless, there has not been a simultaneous, detailed correlation between increased pulsatile pressure and flow and altered wall morphology, composition, and mechanical properties.

In this study, we exploited a mouse model that has been used to study the development of left ventricular hypertrophy [17–19], but also creates very different pulsatile hemodynamics in the right and left common carotid arteries [20]. Following the placement of a fixed diameter band around the aortic arch, between the innominate and left carotid arteries, pulsatility increases significantly in the right carotid while changing slightly in the left, with mean pressure and flow remaining similar to baseline [18,20]. We quantified changes in arterial morphology, composition, and biaxial mechanical properties 5 or 8 weeks after banding, which was expected to yield a nearly steady state adaptive response [21].

Materials and Methods

Banding Surgery

Animal care, surgical procedures, and experimental protocols were approved by the Texas A&M University Institutional Animal Care and Use Committee. Male wild-type mice having a hybrid C57BL/6J and 129Sv background underwent banding surgery at 9 to 10 weeks of age. Specifically, following sedation via an IP injection of a Xylazine/Ketamine cocktail (10 mg/100 mg in 10 ml of sterile water) at 0.1 ml/10 g body mass, hair was removed locally using Nair and 3 rinses with 70% isopropyl alcohol, and buprenorphine (0.03 g) was given IP. A midline incision (from mandible to mid thorax) exposed the trachea and intubation involved passing a 20 or 23 gauge catheter into the trachea, with visual verification while holding the tongue. A ventilator (Harvard Apparatus, MiniVent Respirator) was attached to the catheter and isoflurane (1.5 to 2%) started. A paramedian incision was introduced 1 mm from the sternum and each rib was cut individually to expose the heart and thymus, which was retracted to expose the aorta and carotid arteries. A curved 22 gauge needle with 6-0 suture was passed under the aorta between the carotid arteries, and a 27 gauge (406 μm) "spacer" was placed on the arch prior to securing the ligature. The spacer was then removed, thus leaving the desired stenosis. The chest was closed with 3 to 5 simple interrupted sutures (5-0 silk) followed by skin closure (continuous interlock pattern). The vaporizer was turned off and the animal weaned from the ventilator. Additional buprenorphine (0.03 g) was given subcutaneously at 8 hour intervals following surgery (minimum of 2 additional doses) as needed depending on indications of pain. Additional information on aortic banding can be found in Rockman *et al.* [18] and Li *et al.* [20].

Blood Flow and Pressure

Hemodynamics were measured *in vivo* using a single-channel pulsed Doppler mainframe and 20 MHz ultrasound probe (Indus Instruments) having a resolution of 300 μm. Specifically, at 5 or 8 weeks after surgery, mice were anesthetized using 1.5 to 2% isoflurane at 1.5 LPM, which minimizes effects of anesthesia on hemodynamics [22]. Hypoallergenic, water soluble ultrasound transmission gel (Parker Laboratories) was spread on a small location on the chest

and at the base of the neck, and mean blood velocity was measured both at (ID_{sten} ~406 μm) and near (ID_{aorta} ~875 μm) the aortic band as well as within the right and sten aorta left carotid arteries. Measured velocities enabled volumetric flowrates Q to be estimated based on diameters ($Q=v_{mean}\,\pi d^2/4$) measured during subsequent *in vitro* mechanical testing (below), values of which were synchronized to velocity/diameter tracings by Hartley et al. [23] to characterize the dynamics. Nevertheless, data were interpreted primarily using a Pulsatility Index (*PI*), which non-dimensionalizes measured velocities and thereby minimizes errors that can be introduced in post-facto analysis of flow based on separately measured diameters. This index can be found from maximum, minimum, and mean velocities [16,20]:

$$PI=(v_{max}-v_{min})/v_{mean}. \tag{1}$$

Blood pressure was measured using a tail-cuff transducer and estimated locally at the carotid arteries. An inflation bulb pressurized the tail cuff to systolic pressure P_{sys}, which temporarily blocked blood flow through the caudal artery. Slowly releasing the cuff pressure restored normal blood flow patterns and identified diastolic pressure P_{dias} [24,25]. A Poiseuille relation was used to estimate the pressure drop along the length of the aorta, and thereby estimate blood pressure at the left carotid relative to that at the tail cuff. This pressure drop was small compared to other measurements of importance, however, particularly the pressure drop across the band-induced stenosis. Li *et al.* [20] placed catheters in the left and right carotid arteries to verify experimentally the "simplified Bernoulli equation" (i.e., a control volume energy balance) for pressure drop across a banded mouse aortic arch. Assuming a steady flow, the pressure drop at the peak stenotic jet centerline velocity v_{jet} (cm/s) is

$$\Delta P=4v_{jet}^2. \tag{2}$$

The regression equation found by Li *et al.* [20] relating this equation to catheter based measurements was $\Delta P=(4v_{jet}^2+4.03)/1.02$, which shows a strong correlation despite an offset.

Mean arterial pressure (*MAP*) in both carotids was approximated using the empirical formula [4]

$$MAP=P_{dias}+P_{pulse}/3 \tag{3}$$

with $P_{pulse}=(P_{sys}-P_{dias})$ the local pulse pressure. Comparisons of the true time-averaged mean pressure calculated from [20] (i.e., averaged pressure waveforms across the cardiac cycle) with values computed using equation 3 revealed errors of ~ 4.9% and 8.9% for right and left carotids, respectively, thus indicating the general utility of equation 3.

Mechanical and Functional Testing

Fourteen mice were studied: 7 normal controls and 7 banded. Mice used as true controls were 11.5±1.62 weeks old and weighed 23.8±2.49 g; baseline hemodynamics were measured in a sub-set of this group. Mice banded at 9 to 10 weeks of age were studied at 15.0±1.41 weeks old and weighed 24.6±1.27 g at the time of mechanical testing. Methods for harvesting, mounting, and biaxially testing isolated mouse carotid arteries are in [26] and further details on the testing device are in [27]. Unloaded dimensions (i.e., inner radius R_i, outer radius R_o, and specimen length L) were measured interactively by first identifying the length at which the vessel began to bend at zero pressure; circumferential and axial stretches were calculated

based on these dimensions. Standard preconditioning [26] was used to minimize hysteresis and the *in vivo* axial stretch λ_z^{iv} was estimated. Wall volume, averaged over 12 to 15 measurements of inner and outer radii at multiple static pressures and lengths, remained nearly constant over the short periods of testing (i.e., without growth and remodeling), thus inner radius r_i and wall thickness $h=(r_o-r_i)$ were calculated at any testing state from on-line measurements of outer radius r_o and length ℓ by assuming incompressibility. Mechanical testing consisted of cycling pressure twice from 0 to 140 mmHg at each of three fixed axial stretches $\lambda_z \simeq \lambda_z^{iv}, \lambda_z^{iv+}, \lambda_z^{iv-}$ (i.e., at and ±5% of the *in vivo* value) and cycling axial extension twice at each of three fixed pressures (P = 60, 100, 140 mmHg) while varying the axial load from 0 to 8.8 mN (0.9 g). Pressure-diameter results were interpolated for exact values of λ_z^{iv} found via data analysis after the experiments.

Following mechanical testing, we evaluated endothelial and smooth muscle functionality using methods in [26]. Briefly, phenylephrine (10^{-5} M) was added to the adventitial bath to test smooth muscle contractility, carbamycholine chloride (10^{-5} M) was used to test endothelial-dependent smooth muscle relaxation, and sodium nitroprusside (10^{-4} M) was used to test endothelial-independent relaxation. Only those vessels responding to both vasoconstrictors and vasodilators with at least a uniform change in diameter were considered functional and used for basal smooth muscle condition data. The media was then replaced with Hank's Balanced Salt Solution (HBSS) without calcium and magnesium, but containing sodium nitroprusside (10^{-5} M) and EGTA (2×10^{-3} M) to ensure full smooth muscle relaxation. Biaxial mechanical testing described above was repeated for this passive state.

Mean circumferential and axial wall stresses were estimated by [28]

$$\sigma_\theta=\frac{Pr_i}{r_o-r_i}, \quad \sigma_z=\frac{f_T+P\pi r_i^2}{\pi\left(r_o^2-r_i^2\right)}, \tag{4,5}$$

where P is the transmural pressure and f_T the axial force measured by the transducer. Stretch ratios were calculated at the mid-wall, where $r_{mid}=(r_o+r_i)/2$. Basal or passive circumferential, axial, and radial stretches were calculated via

$$\lambda_\theta=\frac{r_{mid}}{R_{mid}}, \quad \lambda_z=\frac{\ell}{L}, \quad \lambda_r=\frac{1}{\lambda_\theta\lambda_z} \tag{6,7,8}$$

where R and L are radii and axial length, respectively, in the unloaded basal configuration.

Histology

Specimens were removed from the testing device under passive smooth muscle conditions, fixed in 4% paraformaldehyde for 1 hour, and placed in 30% sucrose overnight. They were then put in blocks with OCT and frozen in a beaker of 2-methylbutane placed in liquid nitrogen. Frozen blocks were sectioned at 5 μm from varying locations along the length of the vessel. Sections were mounted on slides and stained using standard hematoxylin and eosin (H&E), Verhoeff-Van Gieson (VVG), picrosirius red (PSR), or Safranin O (with prestaining using Weihert's iron hematoxillin, destaining in fresh acid alcohol, and staining with 0.005% fast green in 1% acetic acid prior to final staining with 0.1% Safranin O). Additional sections were probed with anti-MCP-1 antibody (SC-1785, Santa Cruz Biotechnology) following manufacturer instructions. Sections were incubated with the primary antibody at 1:100 dilution

and the secondary antibody, coupled to the Dylight 488 fluorphore (072-03-13-06, KPL Laboratories), at 1:50 dilution. A negative control for each vessel, with the primary antibody absent, was processed on the same slide. Nuclei were counter-stained with DAPI. Thus, green fluorescence revealed monocyte chemoattractant protein-1 (MCP-1), blue fluorescence revealed nuclei, and red autofluorescence primarily revealed elastin, each imaged with appropriate filters.

H&E, VVG, Safranin O, and PSR brightfield slides were imaged on an Olympus BX/51 microscope under normal light, with a 20× objective, and recorded using an Olympus DP70 digital camera. Hue, saturation, luminescence (HSL) thresholding was used to separate pixels representing constituents of interest [29]. H&E stained slides show connective tissue as pink/red (H=205–50°, S=0.05–1, L=0–1) and nuclei black/blue (H=160–290°, S=0.1–1, L=0–0.5). Blob analysis was used on the pixels meeting the thresholding criteria for nuclei to include adjacent pixels as one blob; the number of blobs was counted as nuclei number. VVG stained sections show collagen and smooth muscle as pink/red (H=300–17°, S=0.04–1, L=0.1–0.9) and elastin as black (H=0–360°, S=0–1, L=0–0.22). Nuclei also showed up blue/black in VVG stained slides and were removed from the total pixel count for elastin by blob analysis. Pixels of elastin were counted and compared to total pixels of tissue to compute area fractions (φ^e). Safranin O stained tissue revealed glycosaminoglycans (GAG) [30], which were similarly quantified (H=173–240°, S=0.09–0.16, L=0.1–0.8) as an area fraction of GAG to other wall constituents (φ^{GAG}). Under normal light (brightfield), PSR stained tissue shows collagen as pink/red (H=300–0°, S=0.06–1, L=0.01–99) and smooth muscle a dull yellow. PSR sections were also imaged under cross-polarized light (darkfield) to observe collagen birefringence [29,31]. The collagen within the brightfield image was used as a mask for the darkfield image, and collagen fibers under cross-polarized light were quantified and separated into red (H=324–2°), orange (H=13–53°), yellow (H=54–72°), or green (H=73–80°) bins [31]. The area fraction of collagen (φ^c) was based on total fibrillar collagen. MCP-1 was revealed based on green pixels with a saturation level greater than 12% and the result was normalized to the overall cross-sectional area found from red autofluorescence.

Statistical Analysis

Outliers were removed from hemodynamic and biomechanical measurements using the quartile method, and hemodynamic and morphological measurements were compared amongst the baseline common carotid artery (CCA), right common carotid artery after banding (RCCA-B), and left common carotid artery after banding (LCCA-B). A Pearson correlation coefficient (r*) identified relationships between hemodynamic measurements and wall properties. Then, the critical value (t) was found for each hemodynamic-mechanical-histological relationship and the probability (p) was calculated based on the Student-t distribution using n-2 degrees of freedom and 2 tails. Comparisons were considered to be significant when $p<0.05$.

Results

It was observed during surgery that the RCCA-B became engorged immediately after banding while the LCCA-B appeared slightly smaller. Hemodynamic data are listed in Table 1. Differences in mean arterial pressure (Figure 1a) were modest amongst the three groups despite a statistically signficant decrease in LCCA-B compared to CCA (p=0.023). In contrast (Figure 1a), pulse pressure was higher in RCCA-B compared to CCA (p=0.048) and particularly LCCA-B (p=0.003). This increase in pulse pressure in RCCA-B resulted from both an increase in systolic pressure and a decrease in diastolic pressure, each relative to control. Systolic pressures measured at an intermediate time following banding surgery (data not shown) were even higher, suggesting a possible initial jump followed by a gradual decrease due to overall vascular compensation; this possibility is consistent with suggestions by others [18,19], but

was not examined further. The pulsatility index (equation 1) was significantly higher in RCCA-B compared to both CCA (p=0.037) and LCCA-B (p<0.001) while mean flow also differed between RCCA-B and both CCA (p=0.007) and LCCA-B (p=0.001) as seen in Figure 1b.

Heart rates were inferred from Fourier analysis of the Doppler measurements; they were less in banded mice (6.09±0.94 Hz) than in baseline controls (7.17±1.28 Hz) under the same sedation, but lacked statistical significance (p=0.169). Upon excision, the RCCA-B appeared grossly larger with an apparently disorganized adventitia (Figure 2b) compared to CCA (Figure 2a) or LCCA-B (Figure 2c). Gentle, yet consistent, tugging with forceps did not remove this outer tissue. Furthermore, the RCCA-B was able to withstand significant bending moments such that the vessel did not bend when held horizontally. Table 1 reveals further that wall thickness was significantly greater in right carotids compared to baseline (p<0.001) while a smaller, but significant, increase was also observed in the left carotids (p<0.001).

Inner diameters were consistently larger in RCCA-B compared to CCA (p<0.001) and LCCA-B (p<0.001) at all pressures under "basal" tone (Figure 3a; Table 1). Interestingly, CCA and LCCA-B diameters were 9% and 16% larger in the passive state compared to their individual basal states; in contrast, there was little difference between passive and basal diameters for RCCA-B. Consistent with this finding, RCCA-B specimens contracted much less in response to 10^{-5} M phenylephrine and similarly relaxed much less in response to 10^{-5} M carbamycholine chloride (e.g., circumferential stretch increased 0.042 in RCCA-B but 0.075 in LCCA-B). RCCA-B specimens relaxed back to their initial basal/passive state in response to 10^{-4} M sodium nitroprusside, however. Figure 4 summarizes circumferential stretches before and after the addition of the vasoreactants, thus revealing decreased vasomotion in the highly pulsatile vessel.

Although both RCCA-B and LCCA-B reached an apparent steady state outer diameter after about 2 weeks (data not shown), circumferential stresses did not return to baseline values by 5 to 8 weeks (Table 1). At individual mean arterial pressures, circumferential stresses in RCCA-B and LCCA-B were both significantly lower than in CCA (p<0.001). Results were similar at a common transmural pressure of 100 mmHg or individual systolic pressures. Stress-stretch plots of averaged data in the basal state and individual *in vivo* axial stretches λ_z^{iv} (not shown) revealed that RCCA-B had a slightly reduced stiffness for a given circumferential stretch than baseline while LCCA-B had a slightly higher stiffness compared to baseline. Once smooth muscle cells were relaxed (data not shown), LCCA-B stress-stretch plots continued to be higher than CCA while RCCA-B were nearly identical to CCA, thus reinforcing the importance of smooth muscle tone in the balance of stress in the circumferential direction.

In contrast, the axial direction exhibited significant changes in mechanical characteristics resulting from altered pulsatility. The *in vivo* axial stretch (λ_z^{iv}), defined as the ratio of in-situ to unloaded length, decreased significantly in the right compared to both control and left carotids (p<0.001; Table 1). The basal *in vivo* force (F_z^{iv}) needed to maintain a vessel at this extension differed similarly (p<0.001) as seen in Table 1. Whereas LCCA-B and CCA had nearly the same force response during cyclic axial stretching, the RCCA-B had a much greater force at all stretches (Figure 3b). Both *in vivo* axial stretch and *in vivo* force were statistically similar between basal and passive states (not shown). Axial stresses were higher in RCCA-B than LCCA-B or CCA for a given stretch, but quickly reached a limit imposed by the force transducer to prevent damage to the vessels.

Altered wall thickness correlated with changes in pulse pressure (r*=0.632; p=0.006) and systolic pressure (r*=0.466; p=0.040) but not mean pressure (r*=0.020; p=0.473) as seen in Figure 5a. Inner diameter, measured at mean arterial pressure (Figure 5b), correlated with both

pulsatility index and mean flow, with a slightly stronger correlation for *PI* ($r^*=0.915$; $p \ll 0.001$) than Q_{mean} ($r^*=0.834$; $p<0.001$). Correlations between inner diameter and flow variables were similar at all pressures tested (i.e., 100 mmHg, systolic, mean, and diastolic). Altered *in vivo* axial stretch correlated inversely with changes in pulse ($r^*=-0.680$; $p=0.005$) and systolic ($r^*=-0.544$; $p=0.027$) pressure, as seen in Figure 5c. Axial stretch also correlated inversely with all flow parameters (not shown) at $p<0.001$. The *in vivo* axial force had a strong negative correlation with pulse pressure ($r^*=-0.582$; $p=0.017$) and pulsatility index *PI* ($r^*=-0.907$; $p<0.001$).

Histological sections revealed that increased wall thickness in RCCA-B was due, in large part, to a proliferation of cells, increase in glycosaminoglycans, and accumulation of collagen (Figure 6). For example, after thresholding and blob analysis, H&E stained sections revealed a 2.2-fold increase in cell nuclei for RCCA-B (578±28) compared to LCCA-B (264±40), which was significant at $p<0.001$. Analysis of Safranin O stained cross-sections yielded a 1.7-fold increase in GAG fractions relative to total tissue (φ^{GAG}) in RCCA-B (0.150±0.023) compared to LCCA-B (0.086±0.008). Whereas VVG stained sections revealed little apparent change in the amount of elastin, confined primarily to the media, brightfield and darkfield PSR stained sections revealed marked increases in fibrillar collagen associated with higher pulsatility, particularly in the adventitia. The associated collagen-to-elastin ratio was thus significantly higher ($p=0.037$) in RCCA-B (1.49±0.261) than in LCCA-B (0.70±0.137), which is seen in Figure 7a. RCCA-B also contained more collagen fibers with green birefreingence (20%), indicating a greater proportion of thinner fibers [31], while less than 10% of LCCA-B fibers were green (Figure 9b). Conversely, LCCA-B contained more thicker orange fibers (34%) compared to the RCCA-B (25%). Adventitial collagen in RCCA-B sections consistently appeared disorganized with marked separations that probably occurred during sectioning and distorted the sections from circular. This separation suggested that much of the newly accumulated adventitial collagen was only loosely incorporated within extant tissue after 5 or 8 weeks of adaptation to the highly pulsatile loading. Finally, there was a significant increase in MCP-1 ($p=0.042$) associated with increased pulsatility (Figure 8). Area fractions for MCP-1 immunostaining based on fluorescence images were RCCA-B (0.855±0.125), LCCA-B (0.014 ±0.007), and CCA (0.032±0.015).

Changes in the total number of cell nuclei (Figure 8) correlated with wall thickness ($r^*=0.826$; $p<0.001$), *in vivo* axial stretch ($r^*=-0.818$; $p<0.001$), and inner diameter ($r^*=0.892$; $p<0.001$). As the wall thickened in response to increased pulsatility (cf. Figure 5a), the area fraction of collagen φ^c ($r^*=0.596$; $p=0.045$) and GAGs φ^{GAG} ($r^*=0.818$; $p=0.007$) increased as seen in Figure 8a. Results were similar for inner diameter (Figure 8b), which also correlated inversely ($r^*=-0.665$; $p=0.018$) with the area fraction of elastin (not shown). Figure 8c also shows that the collagen to elastin ratio and area fraction of GAGs correlated inversely with *in vivo* axial stretch: ($r^*=-0.709$; $p=0.01$) and ($r^*=-0.648$; $p=0.041$), respectively.

Discussion

Arterial growth (change in mass) and remodeling (change in structure) in response to altered dynamic mechanical stimuli may be more important than previously thought. To investigate this possible relationship further, we placed a stiff band around the aortic arch in mice to cause paired carotid arteries to have similar mean pressure and flow, but different pulsatility. We then correlated changes in hemodynamics with long-term (5 or 8 week) changes in wall morphology, composition, and biaxial mechanical responses. Among other findings, increased pulse pressure in the right carotid artery correlated well with dramatic increases in wall thickness and decreases in the *in vivo* axial stretch. This thickening of the wall resulted, in part, from marked increases in cell number, GAG content, and fibrillar collagen, particularly in the adventitia, with the additional collagen fibers appearing thinner and less ordered based on gross

and histological observations. There was also a significant increase in MCP-1, a potent monocyte chemoattractant that is synthesized by multiple vascular cell types and often associated with local inflammatory responses. Inner diameter (measured *in vitro* at mean pressure) also increased significantly in the highly pulsatile right carotid artery, but it correlated only slightly better with the pulsatility index *PI* than with mean flow.

Pulse pressure has been identified as an independent risk factor in human cardiovascular disease [11,13,14], which should not be surprising given that increased systolic pressure promotes cardiac hypertrophy while decreased diastolic pressure can decrease coronary perfusion. Nevertheless, few studies have attempted to quantify *in vivo* dynamic mechanical stimuli more broadly as initiators or indicators of arterial disease. For example, although pulse pressure is known to affect wall thickness in resistance vessels [32–34], few have studied conduit arteries. We found that increased carotid artery wall thickness correlated with increased pulse (r^*=0.632) but not mean (r^*=0.020) pressure. Using a different correlation method (Spearman), Boutouyrie *et al.* [15] similarly found that pulse pressure had a greater effect on intimal-media thickening in human carotids than did mean pressure. Koffi *et al.* [35] also reported a positive correlation between pulse pressure and thickness of thoracic aorta in spontaneously hypertensive rats. They suggested that wall composition, including altered collagen to elastin ratios, can change without any change in mean pressure. Based on available data, therefore, effects of pulse pressure on arterial structure and function may be important both locally and via transmitted effects to distal resistance vessels, thereby contributing to a vicious cycle of vascular stiffening.

Whereas most investigators focus primarily on hypertension-induced changes to the intima and media, most of the growth and remodeling in our mouse model manifested in the adventitia, where stiff collagen fibers serve primarily to prevent acute overstretching of medial smooth muscle cells [1]. Increasing evidence suggests that adventitial fibroblasts play a much greater role in various types of vascular remodeling than long thought [36–39]. Indeed, the marked adventitial remodeling observed herein was accompanied by a particularly higher adventitial cell number in RCCA-B than LCCA-B (0.69±0.07 vs. 0.33±0.045; adventitial/total cell ratio) as well as an increase in the proportion of thinner (green birefringence) and apparently more disorganized collagen fibers. Thinner fibers may be in an incomplete state of assembly or cross-linking and thus may not be capable of bearing load fully. This possibility may suggest that the calculated lower than baseline mean circumferential wall stress in RCCA-B (cf. Table 1) is misleading and there is a need for more sophisticated analyses of the state of stress that account for the evolving make-up of the wall (e.g., via mixture-based constitutive models, [40]), not just changes in loads and geometry (i.e., $\sigma_\theta = P_i r/h$). The lower mean circumferential stress in LCCA-B resulted primarily from a marked decrease in radius at MAP, however, thus emphasizing the complex roles of altered pressure and flow in governing wall mechanics and thus cellular mechanobiological responses.

Comparing our finding of more thinner (green) collagen fibers at 5 or 8 weeks to the finding by Versari et al. [41] of more thicker (red/orange) collagen fibers in porcine carotid arteries at 12 weeks post-surgery in a renovascular model of hypertension suggests that the “maturation” of collagen fibers may take longer than basic geometric changes (cf.[21]). It would thus be of considerable interest to track possible maturation kinetics as well as the probable compaction of more mature fibers by (myo)fibroblasts. Note, therefore, that proteoglycans/glycosaminoglycans influence collagen I fibrillogenesis and thus also merit increased attention. Although it has long been known that hypertension increases proteoglycan content in carotid arteries [42], it appears that we are the first to show an increased accumulation of GAGs (about 1.7-fold) in carotids due primarily to increased pulsatility. This finding is consistent, however, with *in vitro* studies showing that cyclic stretching of other cardiovascular cells increases GAG production about 1.6-fold [43]. Inflammatory mediators can complicate further the kinetics of

turnover of extracellular matrix in response to hypertension. For example, it has been known for many years that MCP-1 is upregulated in hypertensive arteries [44]. Whereas Riou et al. [45] showed in organ culture that MCP-1 expression increases in response to an increase in static pressure alone, Guest et al. [46] showed in smooth muscle cell culture that cyclic 20% strain increases MCP-1 production ~2-fold over static controls. Our results are generally consistent with these prior findings, but appear to be the first to show increased MCP-1 expression *in vivo* due primarily to increased pulsatility. Finally, it should be noted that despite the large increase in wall thickness (e.g., from ~25 μm in CCA to 88 μm in RCCA-B under in vivo conditions), there was no histological indication of increased vasa vasorum. This finding is consistent with that of Versari et al. [41] in hypertensive porcine carotid arteries, which are thicker overall and would be expected to be more sensitive to changes in vasa vasorum.

Blood flow controls arterial caliber, but there has similarly been less attention to effects of pulsatility. Guyton and Hartley [16] found, however, that luminal circumference ratios correlated better with peak velocity and pulsatility index *PI* than with mean velocity in flow-restricted carotid arteries of juvenile rats. Our data partially supports this observation; carotid caliber in the RCCA-B (cf. Figure 3a) correlated slightly better with pulsatile (r^*=0.915) than mean (r^*=0.834) flow. It is well known, of course, that endothelial cells are mechano-sensitive to pulsatile blood flow, that is, cyclic wall shear stress. For example, in vitro tests using cell culture suggest that endothelial gene expression can be more sensitive to unsteady than steady flow and in vivo pathological studies suggest that sites of atherosclerosis correlate with regions of oscillatory as well as low wall shear stress [47–49]. The complexity of endothelial dependence on both mean and pulsatile blood flow was highlighted, however, by an *in vitro* finding on porcine aortic endothelial cells that ~3000 genes were more responsive to changes in mean flow whereas ~232 genes were more responsive to changes in cyclic flow [50]; clearly both aspects of flow are important.

Our biaxial mechanical tests revealed little difference between RCCA-B vessels tested under basal and passive conditions, suggesting that either they were already mostly passive or they were so stiff structurally that smooth muscle relaxation had little effect. Functional tests confirmed that RCCA-B had little contractile capacity, which may suggest a smooth muscle cell transition toward a synthetic phenotype. Following attempted stimulation with phenylephrine, there was also only a modest dilatory response to carbamycholine chloride despite a near full dilatation back to baseline in response to sodium nitroprusside. Because the former acts through the endothelium whereas the latter does not, this suggests possible endothelial dysfunction as well, again consistent with a study on hypertensive porcine carotids [41]. Although we did not evaluate molecular indicators of either smooth muscle cell phenotypic modulation or endothelial dysfunction, Hu et al. [29] found a gradual decrease in contractile markers (smoothlin, calponin) in porcine aortic smooth muscle cells in an aortic coarctation model of hypertension and Ziegler *et al.* [48] found that endothelial cells exposed to complex waveforms of wall shear stress released more endothelin-1 and less nitric oxide. Endothelial changes can be very complex, however, including changes in arginase which competes with eNOS for L-arginine to produce nitric oxide [51]. We did not investigate further the possible causes of the observed diminished functional responses partly because of the significant sectioning damage to the histological slides from the RCCA-B (cf. Figure 6).

The marked decrease in the *in vivo* axial stretch also correlated stronger with pulse pressure than either mean or systolic pressure (cf. Figure 5). Vaishnav et al. [52] reported a similar percent decrease in λ_z^{iv} in a canine model of hypertension, yet this is the first indication that pulse pressure could be the primary mediator. Although there has been little attention to the potentially fundamental aspect of axial remodeling, it is becoming increasingly evident that arterial adaptations involve highly coupled responses to altered circumferential and axial wall stresses as well as wall shear stress [53,54], and reduced axial stretch may be a particularly

effective means by which the arterial wall can reduce circumferential stress in hypertension [55].

Arterial pressures exhibit similar characteristics and magnitudes between mice and humans [56], but other fundamental cardiovascular parameters (e.g., cardiac output, heart rate, aortic diameter) and their by-products follow allometric scaling laws based on body mass [56,57]. Of particular note here, mean values of wall shear stress tend to differ between mice and humans and so too the Womersley number ($\alpha = a\sqrt{\omega/\nu}$, where a is radius, ω the circular frequency related to heart rate, and ν the kinematic viscosity of blood), which is a good metric of pulsatile effects. One must be cautious, therefore, in attempting to extrapolate specific results from mice to potential implications for humans. Nevertheless, our general findings are consistent with those of Boutouyrie *et al.* [15] for patients and, as suggested by Masson *et al.* [58], qualitative findings from biaxial mechanical studies of animal vessels can provide strong guidance for patient-specific modeling and thereby possible interpretation of clinical data.

In conclusion, we presented the first data showing that dramatic alterations in all three primary geometric characteristics of the wall (luminal radius, wall thickness, and axial stretch) correlate stronger with pulsatile rather than with mean pressure and flow. Such adaptations resulted from altered endothelial, smooth muscle, and fibroblast function, with particularly strong adventitial changes and reductions in axial stretch and possible inflammatory contributions mediated by recruited monocytes/macrophages. There is, therefore, a need for a more comprehensive spatial and temporal understanding of arterial adaptations in hypertension, including regional differences within the three primary layers of the arterial wall and thus inherent differences in the associated mechanobiological responses of endothelial cells, smooth muscle cells, fibroblasts, and monocytes. We submit that the complexity of the biomechanics and mechanobiology demands the use of mathematical modeling to integrate the large amounts of data that are becoming available, which must include biaxial data that can reveal potential compensatory roles of changes in axial and circumferential wall mechanics.

Acknowledgments

Kristin Miller, B.S. and Jaclyn Boone provided technical assistance, Jan McCallum, M.S.P.H. provided statistical advice, Andy Ambrus, D.V.M. provided histological expertise, and Drs. Craig Hartley and George Taffet provided valuable guidance on the use of the banding model. This research was supported, in part, by a Bioengineering Research Partnership grant from the NIH (HL-64372).

Partial Funding Source: Bioengineering Research Partnership grant from the NIH (HL-64372)

References

1. Humphrey JD, Na S. Elastodynamics and arterial wall stress. Ann Biomed Eng Apr;2002 30(4):509–523. [PubMed: 12086002]
2. London GM, Guerin AP. Influence of arterial pulse and reflected waves on blood pressure and cardiac function. Am Heart J Sep;1999 138(3 Pt 2):220–224. [PubMed: 10467216]
3. Gaballa MA, Jacob CT, Raya TE, Liu J, Simon B, Goldman S. Large artery remodeling during aging: biaxial passive and active stiffness. Hypertension Sep;1998 32(3):437–443. [PubMed: 9740608]
4. Berne, RM.; Levy, MN. Cardiovascular Physiology. Vol. 8. St. Louis, Missouri: Mosby, Inc; 2001.
5. O'Rourke MF, Hashimoto J. Mechanical factors in arterial aging: a clinical perspective. J Am Coll Cardiol Jul 3;2007 50(1):1–13. [PubMed: 17601538]
6. Jeremy RW, Huang H, Hwa J, McCarron H, Hughes CF, Richards JG. Relation between age, arterial distensibility, and aortic dilatation in the Marfan syndrome. Am J Cardiol Aug 15;1994 74(4):369–373. [PubMed: 8059700]
7. Jondeau G, Boutouyrie P, Lacolley P, et al. Central pulse pressure is a major determinant of ascending aorta dilation in Marfan syndrome. Circulation May 25;1999 99(20):2677–2681. [PubMed: 10338462]

8. Avolio A, Jones D, Tafazzoli-Shadpour M. Quantification of alterations in structure and function of elastin in the arterial media. Hypertension Jul;1998 32(1):170–175. [PubMed: 9674656]
9. Greenwald SE. Ageing of the conduit arteries. J Pathol Jan;2007 211(2):157–172. [PubMed: 17200940]
10. Wagenseil JE, Nerurkar NL, Knutsen RH, Okamoto RJ, Li DY, Mecham RP. Effects of elastin haploinsufficiency on the mechanical behavior of mouse arteries. Am J Physiol Heart Circ Physiol Sep;2005 289(3):H1209–1217. [PubMed: 15863465]
11. Safar ME. Pulse pressure, arterial stiffness, and cardiovascular risk. Curr Opin Cardiol Jul;2000 15 (4):258–263. [PubMed: 11139089]
12. Dart AM, Kingwell BA. Pulse pressure--a review of mechanisms and clinical relevance. J Am Coll Cardiol Mar 15;2001 37(4):975–984. [PubMed: 11263624]
13. Laurent S, Tropeano AI, Boutouyrie P. Pulse pressure reduction and cardiovascular protection. J Hypertens Suppl May;2006 24(3):S13–18. [PubMed: 16723861]
14. Safar ME, Boudier HS. Vascular development, pulse pressure, and the mechanisms of hypertension. Hypertension Jul;2005 46(1):205–209. [PubMed: 15911744]
15. Boutouyrie P, Bussy C, Lacolley P, Girerd X, Laloux B, Laurent S. Association between local pulse pressure, mean blood pressure, and large-artery remodeling. Circulation Sep 28;1999 100(13):1387–1393. [PubMed: 10500038]
16. Guyton JR, Hartley CJ. Flow restriction of one carotid artery in juvenile rats inhibits growth of arterial diameter. Am J Physiol Apr;1985 248(4 Pt 2):H540–546. [PubMed: 3885757]
17. Liao Y, Ishikura F, Beppu S, et al. Echocardiographic assessment of LV hypertrophy and function in aortic-banded mice: necropsy validation. Am J Physiol Heart Circ Physiol May;2002 282 (5):H1703–1708. [PubMed: 11959634]
18. Rockman HA, Knowlton KK, Ross JJ, Chien KR. In vivo murine cardiac hypertrophy: a novel model to identify genetic signaling mechanisms that activate an adaptive physiological response. Circulation 1993;87(suppl VII):VII–14–VII–21.1993
19. Nakamura A, Rokosh DG, Paccanaro M, et al. LV systolic performance improves with development of hypertrophy after transverse aortic constriction in mice. Am J Physiol Heart Circ Physiol Sep; 2001 281(3):H1104–1112. [PubMed: 11514276]
20. Li YH, Reddy AK, Taffet GE, Michael LH, Entman ML, Hartley CJ. Doppler evaluation of peripheral vascular adaptations to transverse aortic banding in mice. Ultrasound Med Biol Sep;2003 29(9): 1281–1289. [PubMed: 14553805]
21. Li YH, Hsieh CY, Wang DL, et al. Remodeling of carotid arteries is associated with increased expression of thrombomodulin in a mouse transverse aortic constriction model. Thromb Haemost Apr;2007 97(4):658–664. [PubMed: 17393030]
22. Janssen BJ, De Celle T, Debets JJ, Brouns AE, Callahan MF, Smith TL. Effects of anesthetics on systemic hemodynamics in mice. Am J Physiol Heart Circ Physiol Oct;2004 287(4):H1618–1624. [PubMed: 15155266]
23. Hartley CJ, Reddy AK, Madala S, Entman ML, Michael LH, Taffet GE. Noninvasive ultrasonic measurement of arterial wall motion in mice. Conf Proc IEEE Eng Med Biol Soc 2004;5:3688–3691. [PubMed: 17271094]
24. Stegall HF, Kardon MB, Kemmerer WT. Indirect measurement of arterial blood pressure by Doppler ultrasonic sphygmomanometry. J Appl Physiol Dec;1968 25(6):793–798. [PubMed: 5727212]
25. Reddy AK, Taffet GE, Madala S, Michael LH, Entman ML, Hartley CJ. Noninvasive blood pressure measurement in mice using pulsed Doppler ultrasound. Ultrasound Med Biol Mar;2003 29(3):379–385. [PubMed: 12706189]
26. Eberth JF, Taucer AI, Wilson E, Humphrey JD. Mechanics of carotid arteries in a mouse model of Marfan syndrome. Ann Biomed Eng Jun;2009 37(6):1093–1104. [PubMed: 19350391]
27. Gleason RL, Gray SP, Wilson E, Humphrey JD. A multiaxial computer-controlled organ culture and biomechanical device for mouse carotid arteries. J Biomech Eng Dec;2004 126(6):787–795. [PubMed: 15796337]
28. Gleason RL, Wilson E, Humphrey JD. Biaxial biomechanical adaptations of mouse carotid arteries cultured at altered axial extension. J Biomech 2007;40(4):766–776. [PubMed: 16750537]

29. Hu JJ, Ambrus A, Fossum TW, Miller MW, Humphrey JD, Wilson E. Time courses of growth and remodeling of porcine aortic media during hypertension: a quantitative immunohistochemical examination. J Histochem Cytochem Apr;2008 56(4):359–370. [PubMed: 18071063]
30. Azeloglu EU, Albro MB, Thimmappa VA, Ateshian GA, Costa KD. Heterogeneous transmural proteoglycan distribution provides a mechanism for regulating residual stresses in the aorta. Am J Physiol Heart Circ Physiol Mar;2008 294(3):H1197–1205. [PubMed: 18156194]
31. Rich L, Whittaker P. Collagen and picrosirius red staining: a polarized light assessment of fibrillar hue and spatial distribution. Braz J Morphol Sci 2005;22(2):97–104.
32. Baumbach GL. Effects of increased pulse pressure on cerebral arterioles. Hypertension Feb;1996 27 (2):159–167. [PubMed: 8567036]
33. Baumbach GL, Siems JE, Heistad DD. Effects of local reduction in pressure on distensibility and composition of cerebral arterioles. Circ Res Feb;1991 68(2):338–351. [PubMed: 1991342]
34. Christensen KL. Reducing pulse pressure in hypertension may normalize small artery structure. Hypertension Dec;1991 18(6):722–727. [PubMed: 1835958]
35. Koffi I, Safar ME, Labat C, Lacolley P, Benetos A, Mourad JJ. Arterial structural changes with verapamil in spontaneously hypertensive rats. Am J Hypertens Jul;1999 12(7):732–738. [PubMed: 10411371]
36. Pagano PJ, Gutterman DD. The adventitia: the outs and ins of vascular disease. Cardiovasc Res Sep 1;2007 75(4):636–639. [PubMed: 17678636]
37. Strauss BH, Rabinovitch M. Adventitial fibroblasts: defining a role in vessel wall remodeling. Am J Respir Cell Mol Biol Jan;2000 22(1):1–3. [PubMed: 10615057]
38. Stenmark KR, Davie N, Frid M, Gerasimovskaya E, Das M. Role of the adventitia in pulmonary vascular remodeling. Physiology (Bethesda) Apr;2006 21:134–145. [PubMed: 16565479]
39. Maiellaro K, Taylor WR. The role of the adventitia in vascular inflammation. Cardiovasc Res Sep 1;2007 75(4):640–648. [PubMed: 17662969]
40. Cardamone L, Valentin A, Eberth JF, Humphrey JD. Origin of axial prestretch and residual stress in arteries. Biomech Model Mechanobiol. Jan 3;2009
41. Versari D, Gossl M, Mannheim D, et al. Hypertension and hypercholesterolemia differentially affect the function and structure of pig carotid artery. Hypertension Dec;2007 50(6):1063–1068. [PubMed: 17968002]
42. Walker-Caprioglio HM, Koob TJ, McGuffee LJ. Proteoglycan synthesis in normotensive and spontaneously hypertensive rat arteries in vitro. Matrix Aug;1992 12(4):308–320. [PubMed: 1435515]
43. Gupta V, Werdenberg JA, Lawrence BD, Mendez JS, Stephens EH, Grande-Allen KJ. Reversible secretion of glycosaminoglycans and proteoglycans by cyclically stretched valvular cells in 3D culture. Ann Biomed Eng Jul;2008 36(7):1092–1103. [PubMed: 18425579]
44. Capers Q, Alexander RW, Lou P, et al. Monocyte chemoattractant protein-1 expression in aortic tissues of hypertensive rats. Hypertension Dec;1997 30(6):1397–1402. [PubMed: 9403559]
45. Riou S, Mees B, Esposito B, et al. High pressure promotes monocyte adhesion to the vascular wall. Circ Res Apr 27;2007 100(8):1226–1233. [PubMed: 17395876]
46. Guest TM, Vlastos G, Alameddine FM, Taylor WR. Mechanoregulation of monocyte chemoattractant protein-1 expression in rat vascular smooth muscle cells. Antioxid Redox Signal Sep-Oct;2006 8 (910):1461–1471. [PubMed: 16987003]
47. Frangos JA, Eskin SG, McIntire LV, Ives CL. Flow effects on prostacyclin production by cultured human endothelial cells. Science Mar 22;1985 227(4693):1477–1479. [PubMed: 3883488]
48. Ziegler T, Bouzourene K, Harrison VJ, Brunner HR, Hayoz D. Influence of oscillatory and unidirectional flow environments on the expression of endothelin and nitric oxide synthase in cultured endothelial cells. Arterioscler Thromb Vasc Biol May;1998 18(5):686–692. [PubMed: 9598825]
49. Gambillara V, Montorzi G, Haziza-Pigeon C, Stergiopulos N, Silacci P. Arterial wall response to ex vivo exposure to oscillatory shear stress. J Vasc Res Nov-Dec;2005 42(6):535–544. [PubMed: 16179795]
50. Himburg HA, Dowd SE, Friedman MH. Frequency-dependent response of the vascular endothelium to pulsatile shear stress. Am J Physiol Heart Circ Physiol Jul;2007 293(1):H645–653. [PubMed: 17322417]

51. Zhang C, Hein TW, Wang W, et al. Upregulation of vascular arginase in hypertension decreases nitric oxide-mediated dilation of coronary arterioles. Hypertension Dec;2004 44(6):935–943. [PubMed: 15492130]

52. Vaishnav RN, Vossoughi J, Patel DJ, Cothran LN, Coleman BR, Ison-Franklin EL. Effect of hypertension on elasticity and geometry of aortic tissue from dogs. J Biomech Eng Feb;1990 112(1): 70–74. [PubMed: 2308306]

53. Dajnowiec D, Langille BL. Arterial adaptations to chronic changes in haemodynamic function: coupling vasomotor tone to structural remodelling. Clin Sci (Lond) Jul;2007 113(1):15–23. [PubMed: 17536999]

54. Humphrey JD. Mechanisms of arterial remodeling in hypertension: coupled roles of wall shear and intramural stress. Hypertension Aug;2008 52(2):195–200. [PubMed: 18541735]

55. Humphrey JD, Eberth JF, Dye WW, Gleason RL. Fundamental role of axial stress in compensatory adaptations by arteries. J Biomech Jan 5;2009 42(1):1–8. [PubMed: 19070860]

56. Westerhof, N.; Stergiopulos, N.; Noble, MIM. Snapshots of hemodynamics: an aid for clinical research and graduate education. New York: Springer; 2005.

57. Weinberg PD, Ethier CR. Twenty-fold difference in hemodynamic wall shear stress between murine and human aorts. Biomechanics Jul;2007 40:1597–1598.

58. Masson I, Boutouyrie P, Laurent S, Humphrey JD, Zidi M. Characterization of arterial wall mechanical behavior and stresses from human clinical data. J Biomech Aug 28;2008 41(12):2618–2627. [PubMed: 18684458]

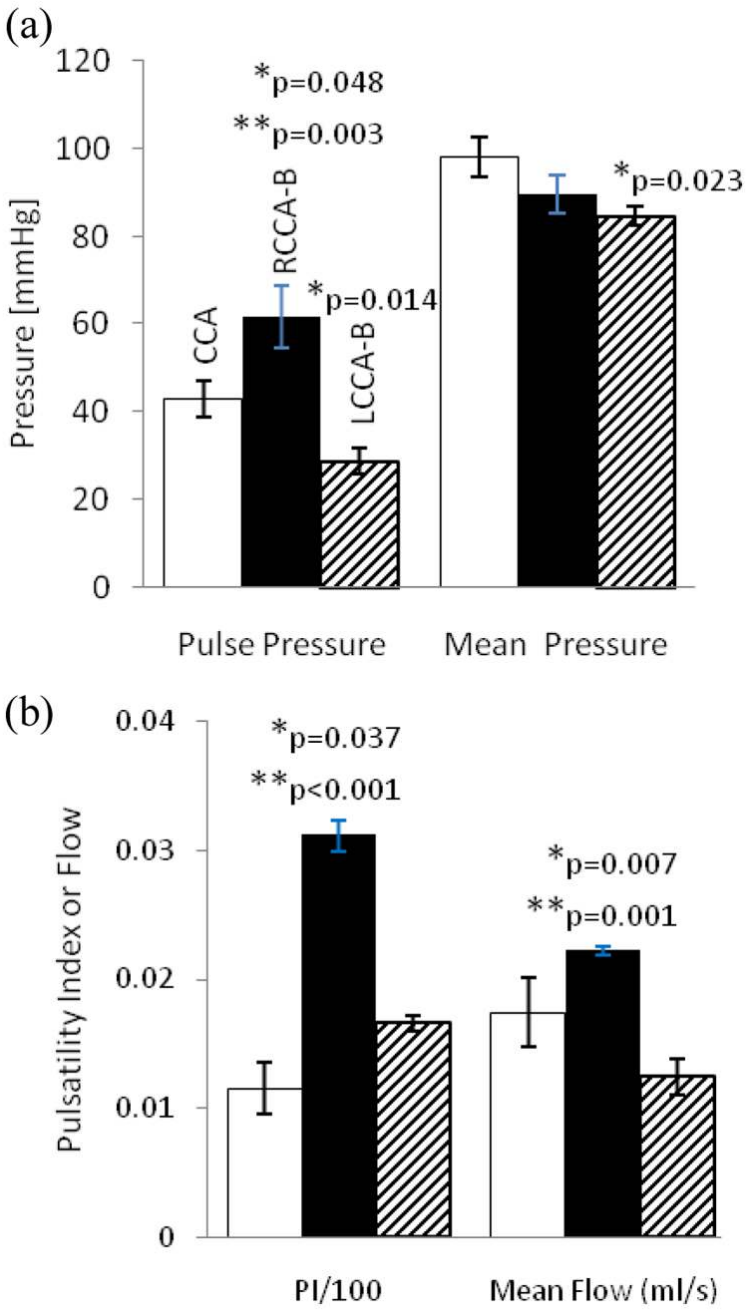

Figure 1.

Hemodynamic measurements for the baseline common carotid artery (□ CCA), right common carotid artery after banding (■ RCCA-B), and left common carotid artery after banding (▨ LCCA-B) for (a) pulse and mean pressure and (b) pulsatility index (PI/100) and mean volumetric blood flow (ml/s). Statistical significance at $p<0.05$ is indicated by (*) for RCCA-B and LCCA-B vessels compared to CCA and by (**) for comparison between RCCA-B and LCCA-B. Bars are standard error of the mean.

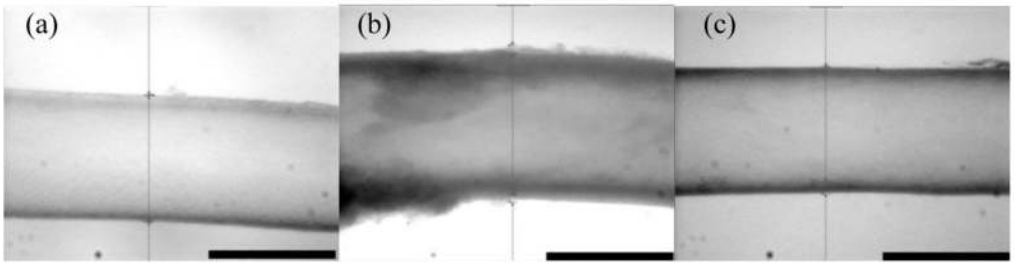

Figure 2.
Video images of mouse common carotid arteries mounted within the mechanical testing device: (a) baseline (CCA), (b) right carotid subjected in vivo to high pulsatile conditions after banding (RCCA-B), and (c) left carotid subjected in vivo to low pulsatile conditions after banding (LCCA-B). Figures are to scale and the black bar represents 660 μm. Vertical lines show video calipers used to measure outer diameters on-line.

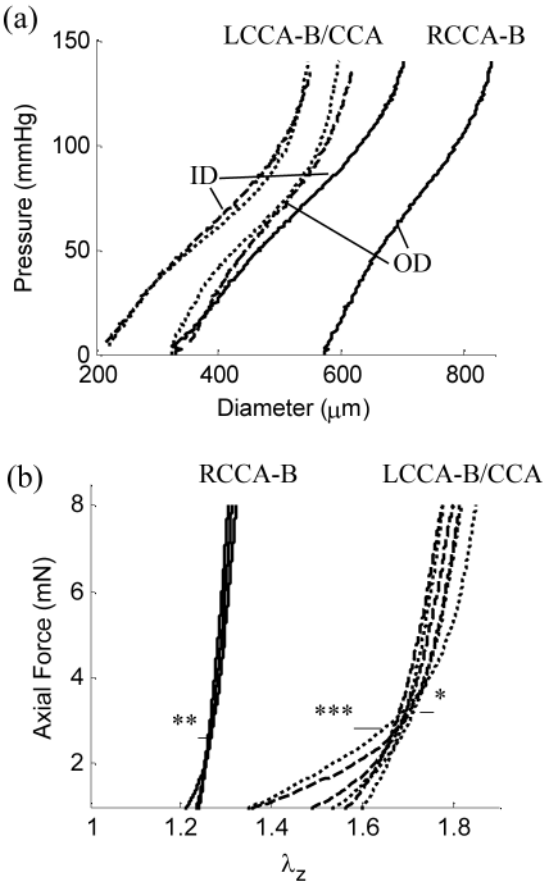

Figure 3.

In vitro (a) pressure-inner diameter (ID) and pressure-outer diameter (OD) behaviors for RCCA-B (—) and LCCA-B (---) after banding and baseline CCA (---). Inner and outer diameters of CCA and LCCA-B were nearly the same while RCCA-B was statistically greater at all pressures. Measured (b) axial force-stretch responses for CCA (---), RCCA-B (—), and LCCA-B (---) at fixed transmural pressures of 60, 100, or 140 mmHg with the location of the *in vivo* axial stretch (crossover point) indicated by *, **, *** for the CCA, RCCA-B, and LCCA-B, respectively.

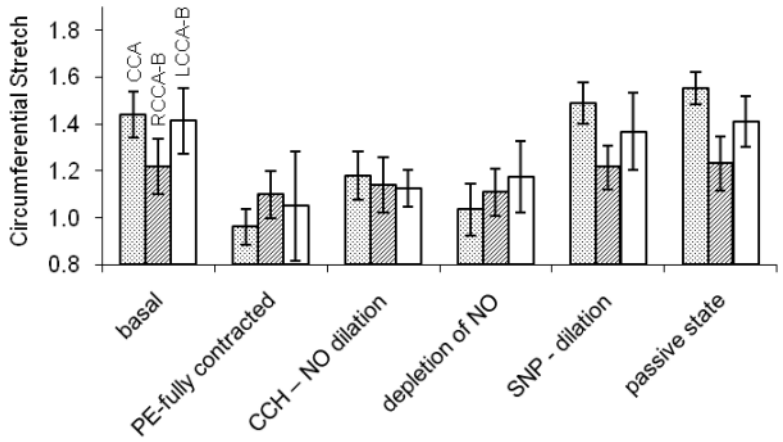

Figure 4.

Circumferential stretch dose-responses for CCA, RCCA-B, and LCCA-B before and after the addition of Phenylephrine (PE) at 10^{-5} M, Carbamycholine chloride (CCH) at 10^{-5} M, Sodium Nitroprusside (SNP) at 10^{-4} M, and calcium and magnesium-free Hank's Balanced Salt Solution (passive state) containing sodium nitroprusside (10^{-5} M) and EGTA (2×10^{-3} M). NO denotes nitric oxide. Error bars represent standard deviation from the mean.

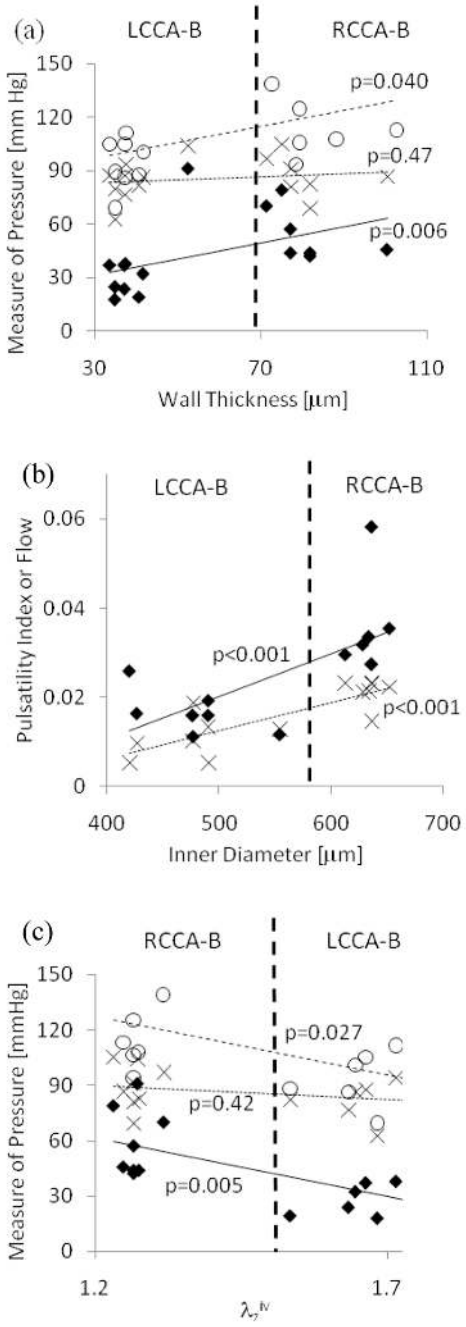

Figure 5.

Relationships between pulsatile (—•—), mean (—×—), or maximum (···o···) pressure and (a) wall thickness or (c) *in vivo* axial stretch (λ_z^{iv}) Relationships between (b) pulsatility index (—•—) or mean volumetric flowrate and (—×—) inner diameter at 100 mmHg. Linear relationships were assumed for consistency with the literature [15,16,35].

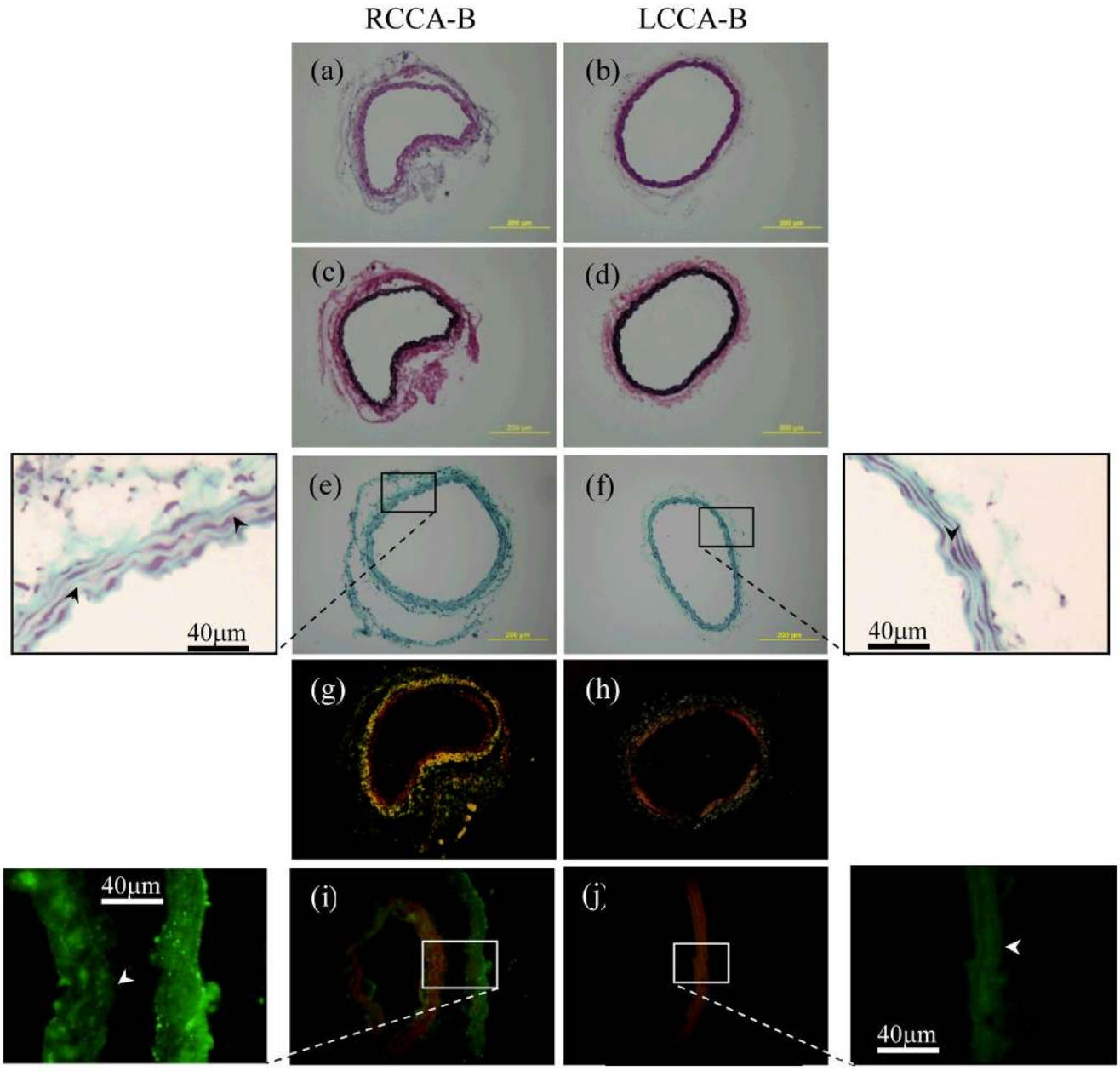

Figure 6.

Representative histological and immunohistochemical sections for RCCA-B and LCCA-B using H&E (a&b) to visualize cell nuclei, VVG (c&d) to visualize elastin, Safranin O (e&f) to visualize glycosaminoglycans (marked by black arrows in 5× enlargements), darkfield PSR (i&j) to visualize fibrillar collagen, and overlaid MCP-1 fluorescence (green) and elastin autofluorescence (red) images (k&l), with 5 × enlargements of immunofluorescent MCP-1 alone and white arrows showing the location of the external elastic lamina. Note the significantly thicker, but disorganized, adventitial layer in the RCCA-B vessels.

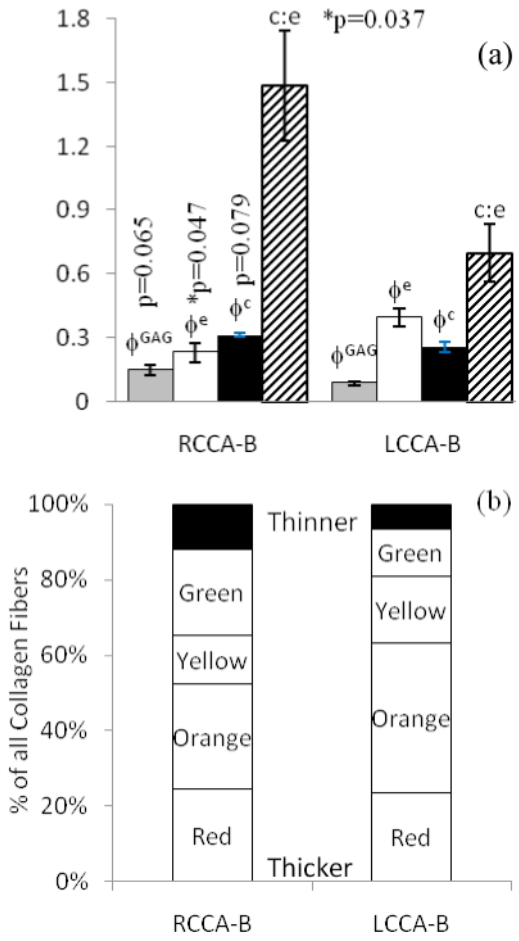

Figure 7.

Histological quantification of (a) GAG area fraction (▨ φ^{GAG}), elastin area fraction (□ φ^{e}), collagen area fraction (■ φ^{c}), and collagen-to-elastin ratio (▨ c:e), as well as (b) color of collagen birefringence [31] in the RCCA-B and LCCA-B. Statistical significance between RCCA-B and LCCA-B at $p<0.05$ is indicated by (*) for Figure 7a. Bars represent standard error of the mean. Note, in particular, the significantly higher c:e for RCCA-B (1.49±0.261) than LCCA-B (0.570±0.059) and the greater percentage of thinner collagen fibers (Yellow/Green) in RCCA-B.

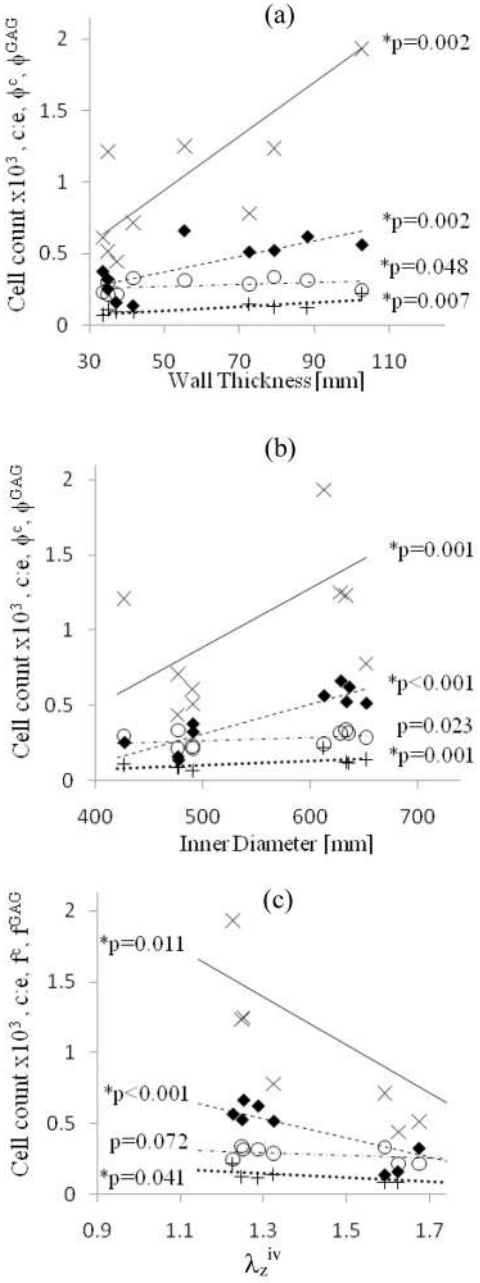

Figure 8.

Correlations amongst histologically measured wall constituents, including cell count ×1000 (), collagen to elastin ratio (), collagen cross sectional area fraction (φ^{c}) (), and GAG cross sectional area fraction (φ^{GAG}) () and macroscopic arterial wall properties: (a) wall thickness, (b) inner diameter at 100 mmHg, and (c) *in vivo* axial stretch.

Table 1

Hemodynamic, morphological, and mechanical parameters measured from baseline control (CCA) or 5-8 weeks after transverse aortic banding.

	CCA	RCCA-B	LCCA-B
P_{sys} (mmHg)*	120±1.91	124±8.42	94.6±4.86
P_{dias} (mmHg)*	77.5±3.26	67.7±1.41	67.9±1.32
Pulsatility Index PI */**	1.16±0.20	3.11±0.12	1.65±0.064
Q_{mean} (ml/s)*/**	0.016±0.003	0.022±0.003	0.012±0.001
h (microns) @ in vivo state*/**	24.8±0.878	88.1±3.86	41.6±0.815
λ_z^{iv} @ in vivo state*/**	1.72±0.029	1.27±0.004	1.67±0.029
f^{iv} (mN) @ in vivo state*/**	3.47±0.137	2.16±0.042	2.68±0.035
$2r_i$ (microns) @ *MAP**/**	484±8.51	591±13.5	410±2.77
$2r_i$ (microns) @ *100 mmHg**/**	496±8.92	633±1.23	482±3.39
σ_θ (kPa) @ *MAP**	124±4.03	44.8±5.76	53.1±1.26
σ_θ (kPa) @ *100 mmHg**/**	137±1.69	56.9±0.72	90.6±2.39

RCCA-B denotes the right common carotid artery after banding that experienced increased pulsatility whereas LCCA-B denotes the left common carotid artery after banding that experienced near normal hemodynamics. Statistical significance at $p<0.05$ is indicated by (*) for RCCA-B and LCCA-B vessels compared to CCA and by (**) for comparison between RCCA-B and LCCA-B. Values are mean ± standard error of the mean.